Supplementary Materials

Iron(IV)hydroxide pKa and the Role of Thiolate Ligation in C-H Bond Activation by Cytochrome P450

Timothy H. Yosca; Jonathan Rittle; Courtney M. Krest; Elizabeth L. Onderko; Alexey Silakov; Julio C. Calixto; Rachel K. Behan, and Michael T. Green*

The Department of Chemistry, Pennsylvania State University, University Park, PA 16802

Contents

I. Materials and Methods

Materials. *m*-CPBA (<77%, Aldrich) was purified to 99%.(*57*) For kinetic studies, solutions of *m*-CPBA were prepared by dissolving *m*-CPBA in acetonitrile and then diluting in water. The maximum final concentration of acetonitrile was 0.1% (v/v). ^{57}Fe-enriched CYP158(A2), with a His4-tag at the C-terminus, was obtained from overexpression in Rosetta Blue (DE3) pLysS (Novagen) competent cells (pET 17b vector, kindly provided by Prof. Michael R. Waterman). These cultures were grown in M9 minimal media supplemented with thiamine and proline (1g of each per 3L culture). At an O. D. of 0.8, protein expression was induced with 0.5 mM IPTG. At the time of expression, 1-2 mg/L of $^{57}FeCl_3$, 0.5 mM δ-aminolevulinic acid, and 1 mL/L of a solution of trace elements ($ZnCl_2 \bullet 4H_2O$, 1 g; $CoCl_2 \bullet 6H_2O$, 0.2 g; $Na_2MoO_4 \bullet 2H_2O$, 1 g; $CaCl_2 \bullet 2H_2O$, 0.5 g; $CuCl_2$, 1 g; and H_3BO_3, 0.2 g in 1 L of 10% HCl) were added to the cultures.

After 24 hours, the cells were harvested, redissolved in buffer (50 mM tris-HCl, pH 7.5, 500 mM NaCl, 10% (v/v) glycerol, and 3 mM imidazole), and lysed using a microfluidizer processor (M-110EH-30). The protein was loaded onto a metal (Ni^{2+}) affinity column (Qiagen) and washed with 2-3 column volumes of lysis buffer. CYP158 was then eluted with buffer containing 50 mM tris-HCl, pH 7.5, 10% (v/v) glycerol, and 80 mM imidazole. Further purification was performed by Q sepharose chromatography (GE Healthcare). Protein was washed with 2 column volumes of buffer containing 20 mM tris-HCl, pH 7.5. CYP158 was eluted using a 0-500 mM NaCl gradient of the same buffer. Fractions with an R_z ($A_{416/280}$) greater than 1.8 were pooled for size exclusion (S-100) chromatography (GE Healthcare) in 20 mM tris-HCl buffer, pH 7.5. CYP158 with an R_z greater than 2.0 was used for experiments.

Freeze-Quenched Samples. Freeze-quench methods were used to generate the iron(IV)hydroxide and iron(IV)oxo intermediates in P450 CYP158. A four syringe ram freeze-quench apparatus from Update Instruments (Madison, WI) was used for all freeze-quench experiments. Aqueous reaction mixtures were sprayed into liquid ethane (89 K). Liquid ethane was subsequently removed under vacuum in an

isopentane bath (~ 120 K), and samples for EPR, Mössbauer, and EXAFS were packed under liquid nitrogen.

1) Preparation of CYP158-II at pH 9. Ferric CYP158 (6 mM) was reacted with *m*-CPBA (60 mM) in a 2:1 mixture (v/v) to form compound II hydroxide. CYP158 was in tris-HCl buffer (100 mM, pH 9) and *m*-CPBA was in a 30% (v/v) solution of acetonitrile. Reactants were mixed and quenched into liquid ethane 3.5 ms after mixing. Samples were packed into Mössbauer sample cups for spectroscopic analysis at a final protein concentration of 4 mM. The final concentrations of *m*-CPBA and acetonitrile were 20 mM and 10% (v/v) respectively.

2) Preparation of CYP158-II at varying pH. Samples were prepared using a three syringe, double mix setup. Ferric CYP158 (6 mM) was reacted with *m*-CPBA (60 mM) in a 2:1 mixture (v/v) to form compound II hydroxide. CYP158 was in tris-HCl buffer (20 mM, pH 9) and *m*-CPBA was in a 40% solution of acetonitrile/water (v/v). Compound II hydroxide was then reacted in a subsequent 3:1 mixture with an arginine HCl/sodium hydroxide buffer (pH 14). The strength of the buffer was varied (10 mM – 108.16 mM) to change the final pH of the solution, thus altering the ratio of compound II oxo/hydroxide. The reaction was quenched in a liquid ethane bath 7 ms after the initial formation of compound II. Portions of the quenched samples were set aside to confirm the final pH of the solution. Samples were packed into Mössbauer sample cups for spectroscopic analysis at a final protein concentration of 3 mM. The final concentrations of *m*-CPBA and acetonitrile were 15 mM and 10% (v/v) respectively.

Mössbauer Spectroscopy. A spectrometer from WEB Research (Edina, MN) was used to collect data in constant acceleration mode with a transmission geometry. Spectra were recorded with a 54 mT magnetic field applied parallel to the γ-beam. All measurements were recorded at 4.2 K using a Janis SVT400 cryostat. Isomer shifts were calibrated relative to the centroid of the spectrum of a metallic foil of α-Fe at room temperature. Data analysis was performed using the program WMOSS from WEB research.

Stopped-Flow Spectrophotometry. Experimental details are given in the legend of Figure 2. Spectral changes were monitored using an SFM-400 stopped flow spectrometer (Bio-Logic SA, Claix, France). The minimum dead time of the instrument is 1.6 ms. An L7893 light source (Hamamatsu, Tokyo, Japan) and a TIDAS photodiode (J&M GmbH, Essingen, Germany) were used to collect absorption data. All experiments were performed at 4°C.

X-Ray Absorption Spectroscopy (XAS). XAS data were collected in fluorescence mode at ~ 10 K with a 30-element germanium detector (SSRL, BL7-3) using a Si(220) Φ = 90° double monochromator with a 9.5 keV cutoff for harmonic rejection. To minimize the effects of photoreduction, samples were moved in the beam so that an unexposed portion of the sample was examined during each set of measurements (exposure time ~ 30min per scan). XAS were obtained by averaging 54 total first scans for CYP158-II hydroxide, 44 first scans of CYP158-II oxo, and 11 first scans for ferric CYP158. The effects of photoreduction were monitored via the analysis of data obtained during the second acquisition scan. Background removal and curve fitting were performed with EXAFSPAK (available at http://www.ssrl.slac.stanford.edu/exafspak.html) using *ab initio* phases and amplitudes generated with FEFF version 8.0. Data sets were fit over the range k = 3 – 15 $Å^{-1}$. Coordination numbers, N, were constrained during the fits. Fits included first and 2nd shell atoms and one multiple scattering component. In all cases, the 2nd shell was comprised of α- and *meso*-carbons and the Fe-C_α–N-Fe multiple scattering paths (n = 8, 4, and 16 respectively). All distances, R, and Debye-Waller factors, σ^2, were treated as adjustable parameters, and all threshold energy shifts, E_o, were linked but allowed to vary. The passive electron reduction factor, S_o, was fixed at 0.9. Edge energies were calibrated using α-Fe metal foil (7111.3 eV). Edge positions were obtained from the first derivative of the data using EXAFSPAK (1.0 eV smoothing, third order polynomial).

Computations. The computational model (fig. S12) was taken from the crystal structure of CYP158.(*27,* PDB accession code: 1S1F) The geometry of the $CH_2SFeO(H)$ unit and the tyrosine were allowed to optimize (the CH2 of the tyrosine was fixed). Everything else was locked in place. Energies for protonation of the iron(IV)oxo moiety with and without the tyrosine oxidized were determined. All calculations were performed with Gaussian 09 at the B3LYP/6-311G level, using implicit solvation.(*60)*

Electron Paramagnetic Resonance (EPR). CW EPR measurements were acquired on a Bruker Elexsys E580 X-band spectrometer equipped with a SuperX-FT microwave bridge. Continuous-wave EPR

measurements were performed using an ER 4122 SHQE SuperX high-sensitivity cavity in combination with an ER 4112-HV Oxford Instruments variable temperature helium flow cryostat.

Q-band spectra were acquired using a home built intermediate frequency (IF) extension of the SuperX-FT X-band bridge as a part of the Bruker X-band ELEXSYS 580 system. In these experiments, we have used a home built TE011 open resonator based on the design of Annino et al (*58*) and constructed similarly to the one presented by Reijerse et al (*59*) in concert with an Oxford CF935 helium flow cryostat. Using Millitech 3W pulsed power amplifier and such a resonator a 12 ns MW $\pi/2$ pulse can be achieved at 10K. However, to obtain better spectral resolution, in this work the incident power was attenuated to obtain T($\pi/2$) ~20ns. Acquisition and experimental control was performed using standard Bruker XEPR software.

II. The Derivation of Equation 7.

If $\frac{\Delta G}{2\gamma}$ is small, then

$$\frac{(\Delta G+\gamma)^2}{4\gamma RT} \cong \frac{\gamma}{4RT} + \frac{\Delta G}{2RT} \qquad \text{(Eq. S1)}$$

So Eq. 5 becomes

$$k = \left(Ae^{-\gamma/4RT}\right)e^{-\Delta G/2RT} \qquad \text{(Eq. S2)}$$

or

$$k = Be^{-\Delta G/2RT} \qquad \text{(Eq. S3)}$$

$$\ln(k) = \ln(B) - \frac{\Delta G}{2RT} \qquad \text{(Eq. S4)}$$

Eq. S4 expresses a linear free energy relationship between the rate constant for non-productive oxidations and the driving force for tyrosine oxidation by compound I. The driving force for this oxidation is given by

$$\Delta G = -23.06\,(E^0_{comp-I} - E^{0\prime}_{Tyr}) \qquad \text{(Eq. S5, rearrange to obtain Eq. 3 in main text)}$$

To obtain Eq. 7, we now consider non-productive oxidations by two different compound I species that are contained in otherwise identical protein environments. We assume that the same intrinsic barriers and donor-acceptor couplings (contained in the B term) will govern non-productive oxidations in these otherwise identical systems.

$$\frac{k_1}{k_2} = \frac{Be^{-\Delta G_1/2RT}}{Be^{-\Delta G_2/2RT}} = e^{-(\Delta G_1 - \Delta G_2)/2RT} \qquad \text{(Eq. S6)}$$

$$\ln\frac{k_1}{k_2} = -(\Delta G_1 - \Delta G_2)/2RT \qquad \text{(Eq. S7)}$$

In order to evaluate Eq. S7 we need to determine the difference between the ΔG's.

$$\Delta\Delta G = \Delta G_2 - \Delta G_1 \qquad \text{(Eq. S8)}$$

Using Eq. S5 and Eq. S8 we obtain

$$\Delta\Delta G = -23.06\,(E^0_{comp-I_{(2)}} - E^0_{comp-I_{(1)}}) \qquad \text{(Eq. S9)}$$

By rearranging Eq. S10, the equation for D(O-H) of compound II,

$$\text{D(O-H)} = [23.06 * E^0_{comp-I} + 2.303RT * pKa + C]\ \text{kcal/mol} \qquad \text{(Eq. S10)}$$

we can obtain Eq. S11, which gives the reduction potential of compound I.

$-23.06 * E^0_{comp-I} = [-\text{D(O-H)} + 2.303RT * pKa + C]$ kcal/mol (Eq. S11)

where C is a constant that depends upon the solvent and reference electrode. Its value is 57.6 ± 2 kcal/mol for aqueous solution with E^0 versus NHE.

Substitution of Eq. S11 into Eq. S9 yields

$\Delta\Delta G = 2.303RT(pKa_2 - pKa_1)$ (Eq. S12)

or

$\Delta\Delta G = 2.303RT(\Delta pKa)$ (Eq. S13)

From Eq. S8, Eq. S9, and Eq. S13 one can then obtain

$\ln\frac{k_1}{k_2} = \Delta\Delta G/2RT$ (Eq. S14)

$\ln\frac{k_1}{k_2} = \frac{2.303RT*\Delta pKa}{2RT}$ (Eq. S15)

$\ln\frac{k_1}{k_2} = \frac{\ln(10)\Delta pKa}{2}$ (Eq. S16)

$\frac{k_1}{k_2} = e^{\frac{\ln(10)\Delta pKa}{2}}$ (Eq. S17)

$\frac{k_1}{k_2} = (e^{\ln(10)})^{\frac{\Delta pKa}{2}}$ (Eq. S18)

$\frac{k_1}{k_2} = 10^{(\frac{\Delta pKa}{2})}$ (Eq. S19, Eq. 7 in main text)

III. The Relative Free Energies of the Productive and Non-Productive Pathways.

The difference between the free energies of the productive and non-productive pathways is given by

$\Delta G_{rel} = \Delta G_p - \Delta G_{np}$ (Eq. S20, Eq. 4 in main text)

The free energy of the product pathway is given by Eq. S21, where D(O-H) is given by Eq. S10 and D(C-H) is the strength of the substrate's C-H bond.

$\Delta G_p = \text{D(C-H)} - \text{D(O-H)}$ (Eq. S21, Eq. 1 in main text)

Using Eq. S5 and Eq. S11, the free energy of the non-productive pathway can be expressed as

$\Delta G_{np} = (-\text{D(O-H)} + 1.37 * pKa + 57.6 \pm 2) + 23.06 * E^{0\prime}_{Tyr}$ kcal/mol (Eq. S22)

So

$\Delta G_{rel} = [\text{D(C-H)} - \text{D(O-H)}] - [-\text{D(O-H)} + 1.37 * pKa + 57.6 \pm 2 + 23.06 * E^{0\prime}_{Tyr}]$ kcal/mol (Eq. S23)

$\Delta G_{rel} = [\text{D(C-H)} - \text{D(O-H)}] + [\text{D(O-H)} - 1.37 * pKa - 57.6 \pm 2 - 23.06 * E^{0\prime}_{Tyr}]$ kcal/mol (Eq. S24)

$\Delta G_{rel} = [\text{D(C-H)} - 1.37 * pKa - 57.6 \pm 2 - 23.06 * E^{0\prime}_{Tyr}]$ kcal/mol (Eq. S25)

Assuming D(C-H) = 101 kcal/mol (BDFE) for an unactivated C-H bond and $E^{0\prime}_{Tyr} = 1.05\ V$ (the average the aqueous tyrosine potentials) for the proton coupled oxidation of tyrosine gives,

$\Delta G_{rel} = [19.19 - 1.37 * pKa \pm 2]$ kcal/mol (Eq. S26)

Eq. S26 reveals that a change of 8.5 units in the compound II pKa corresponds to a shift of 11.6 kcal/mol in the relative free energies of the productive and non-productive pathways.

When $\Delta G_{rel} < 0$ the productive pathway is preferred.

$$\Delta G_{rel} = 19.19 - 1.37 * pKa \pm 2\ kcal/mol < 0 \quad \text{(Eq. S27)}$$

$$-1.37 * pKa < -19.19 \pm 2\ kcal/mol \quad \text{(Eq. S28)}$$

$$pKa > 14.0 \pm 1.5 \quad \text{(Eq. S29)}$$

So, for $E^{0\prime}_{Tyr} = 1.05\ V$, the productive pathway is thermodynamically favored when the compound II pKa > 14.0 ± 1.5.

IV. EXAFS Fitting Results — CYP158-II Hydroxide (pH 9.0)

Table S.1: EXAFS fitting results for CYP158-II hydroxide (pH 9.0).

Fe-N			Fe-S			Fe-O				
N	R	σ^2	N	R	σ^2	N	R	σ^2	E_0	Error
4	**1.99**	**0.001**	**1**	**2.26**	**0.003**	**1**	**1.84**	**0.001**	**-14.6**	**0.281**
4	1.99	0.002	0			1	1.85	0.003	-15.8	0.427
4	2.00	0.002	1	2.29	0.003	0			-10.7	0.339
4	1.99	0.002	0			0			-12.8	0.449

Raw data were fit over the region k = 3-15 Å^{-1}. Coordination number N, interatomic distance R (Å), mean square deviation in R (the Debye-Waller factor), σ^2 (Å^2), and the threshold energy shift E_0 (eV). The fit error is defined as $[\Sigma k^6(\chi_{exptl} - \chi_{calc})^2 / \Sigma k^6 \chi^2_{exptl}]^{1/2}$. Best fits are shown in boldface. Alternative fits with different coordination numbers are shown also. Coordination numbers, N, were constrained during the fits.

V. EXAFS Fitting Results — CYP158-II Oxo (pH 13.3)

Table S.2: EXAFS fitting results for CYP158-II oxo (pH 13.3).

Fe-N			Fe-S			Fe-O				
N	R	σ^2	N	R	σ^2	N	R	σ^2	E_0	Error
4	**2.00**	**0.001**	**1**	**2.36**	**0.009**	**1**	**1.68**	**0.005**	**-13.1**	**0.334**
4	1.99	0.001	0			1	1.69	0.006	-17.0	0.352
4	2.00	0.001	1	2.38	0.009	0			-13.7	0.390
4	2.00	0.001	0			0			-16.3	0.391

Raw data were fit over the region k = 3-15 Å^{-1}. Coordination number N, interatomic distance R (Å), mean square deviation in R (the Debye-Waller factor), σ^2 (Å^2), and the threshold energy shift E_0 (eV). The fit error is defined as $[\Sigma k^6(\chi_{exptl} - \chi_{calc})^2 / \Sigma k^6 \chi^2_{exptl}]^{1/2}$. Best fits are shown in boldface. Alternative fits with different coordination numbers are shown also. Coordination numbers, N, were constrained during the fits.

VI. CYP158-II Formation (Stopped-Flow) at pH 9 and Mössbauer Fits at Varying pH

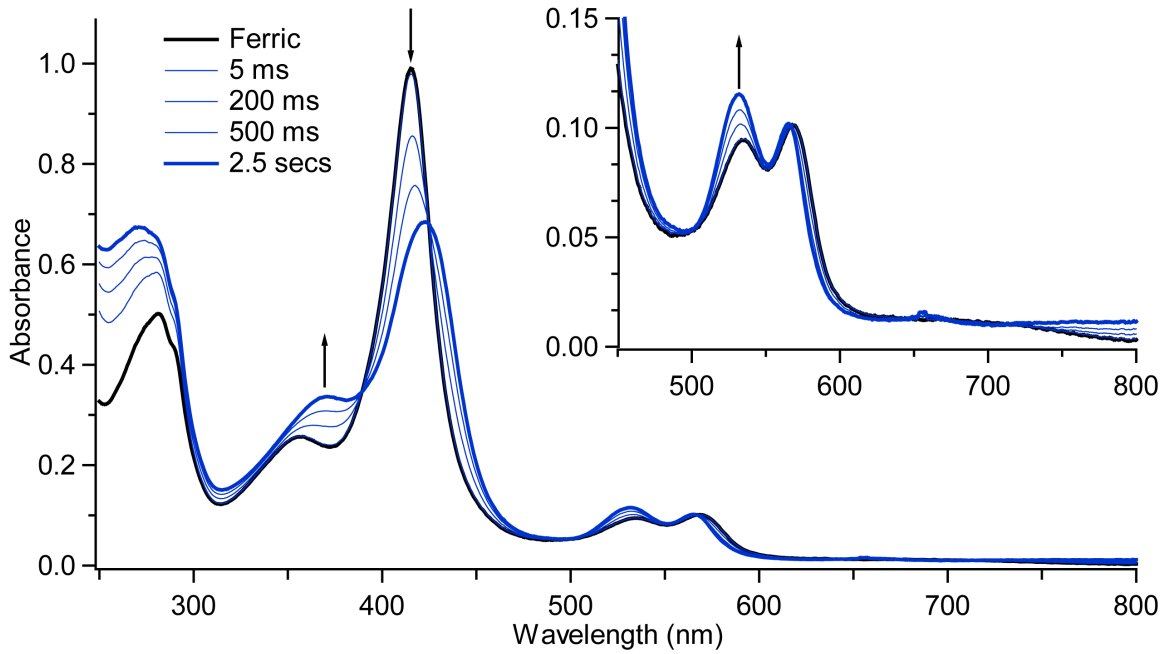

Figure S1: UV/visible spectra obtained from the stopped-flow mixing (1:1) of 20 μM ferric CYP158 (100 mM tris-HCl. pH 9) with 100 μM *m*-CPBA at 4°C. The blue traces correspond to spectra taken at 5, 200, 500, and 2500 ms after mixing. Maximum yield of CYP158-II was at 2.5 seconds.

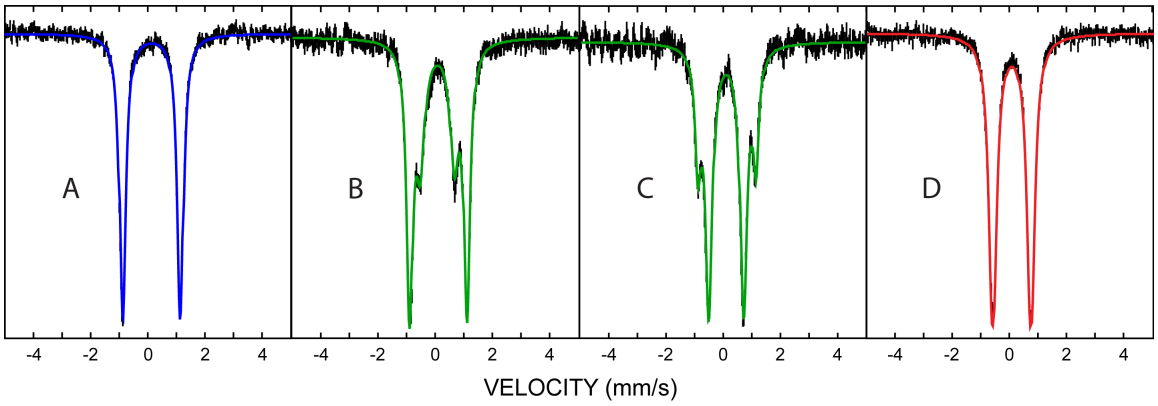

Figure S2: Mössbauer spectra and fits of CYP158-II at varying pH. (A) pH 9.0 (B) pH 11.8 (C) pH 12.2 (D) pH 13.3. The contribution of ferric enzyme (~10-20%) was subtracted from each spectrum. The fits for the intermediate pH's (B) and (C) were obtained by optimizing the ratio of two simulated quadrupole doublets (one with compound II hydroxide parameters σ = 0.10/ΔEq = 2.02 mm/s and one with compound II oxo parameters σ = 0.09/ΔEq = 1.30 mm/s). The relative area (hydroxide/oxo) of each quadrupole doublet is 64%/36% for (B) and 25%/75% for (C). (A) and (D) are representative Mössbauer spectra for the samples analyzed by EXAFS. Compound II hydroxide (A) was prepared in 90% yield while the compound II oxo (D) was prepared in 85% yield.

VII. CYP158-II: Consecutive 100 ms Spectral Averages and Decay Rates at Varying pH.

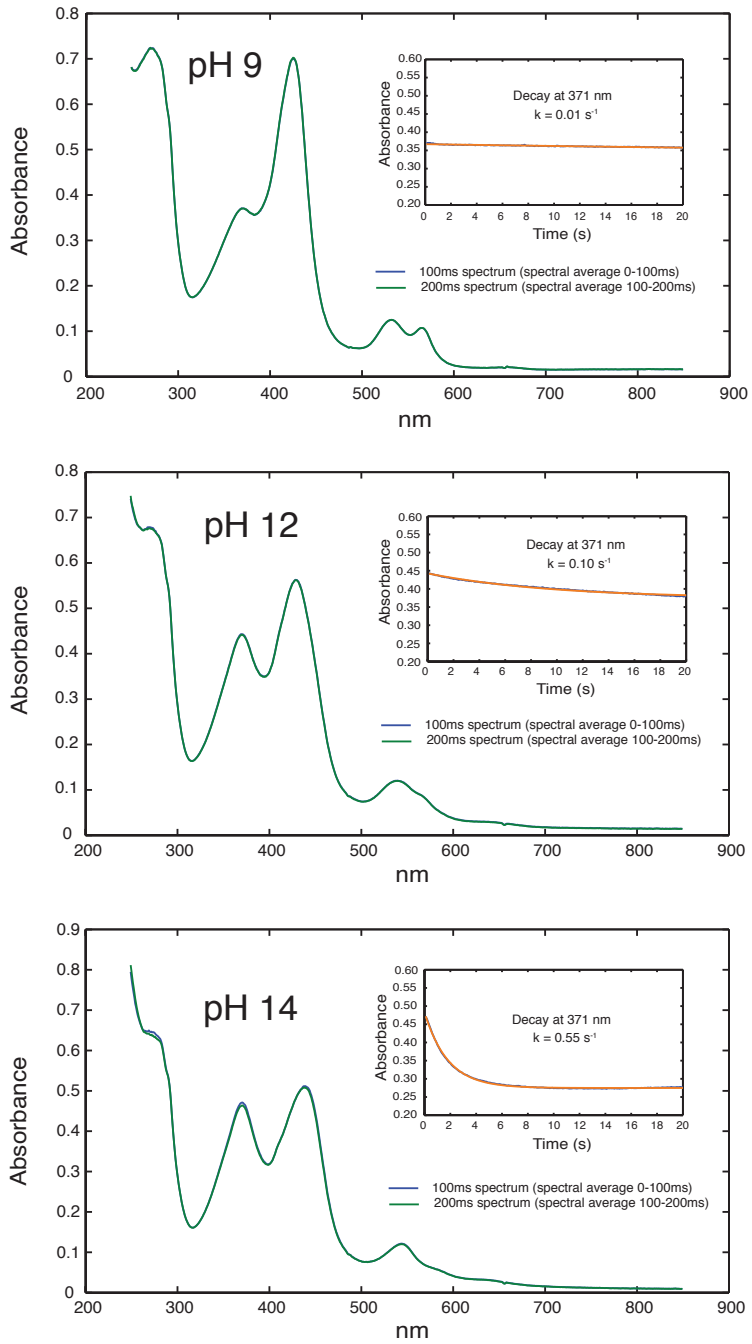

Figure S3: CYP158-II decay. Figures show consecutive 100ms spectral averages. Insets show decay and single exponential fits at 371 nm.

VIII. CYP158-II Reversibility Study - Triple Mix - Low to High to Low pH Jump

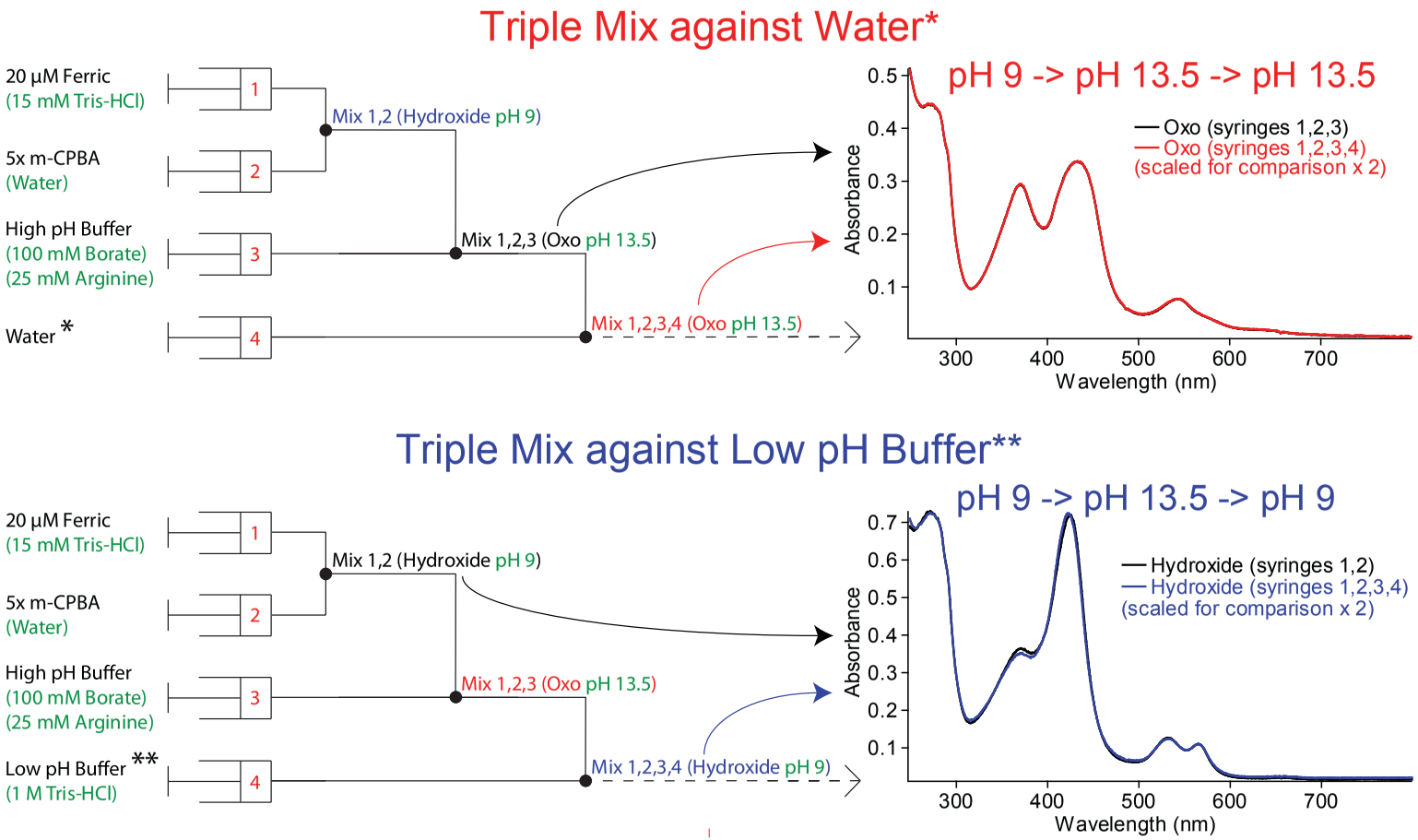

Figure S4: Triple-mix stopped-flow reversibility study of CYP158-II hydroxo to oxo reaction. A triple-mix stopped-flow experiment was used to confirm the reversible nature of the deprotonation event occurring at pH ~ 12. In the control (top) 20 µM ferric protein (15 mM tris-HCl, pH 9) was pre-mixed with 5 equivalents (100 µM) of *m*-CPBA (in water) and held until maximum formation of compound II hydroxide (Fe^{IV}-OH) was achieved (2.5 seconds). The solution was then further mixed with a high pH buffer solution (containing 100 mM Borate, 25 mM arginine, pH 13.5) to generate compound II oxo (Fe^{IV}=O). For the control, a third sequential mix in water was added to show that the compound II oxo spectrum remains unchanged over the timescale required for a third mix, ~ 10 ms. A scaled overlay (top right) shows that the oxo spectrum is essentially identical both before (black) and after (red) a third mix. For the experiment (bottom) the first two mixes were performed as before. The third mix was used to bring the protein solution back to pH 9. This was done using a low pH buffer solution (containing 1 M tris-HCl, pH 7.5). A comparison of the spectra both before (black) and after (blue) the high pH excursion is shown in the bottom right. This experiment confirms the reversibility of the iron(IV)hydroxide deprotonation. All spectra were collected within 2.5 ms of mixing and all mixes were performed in a 1:1:1:1 ratio.

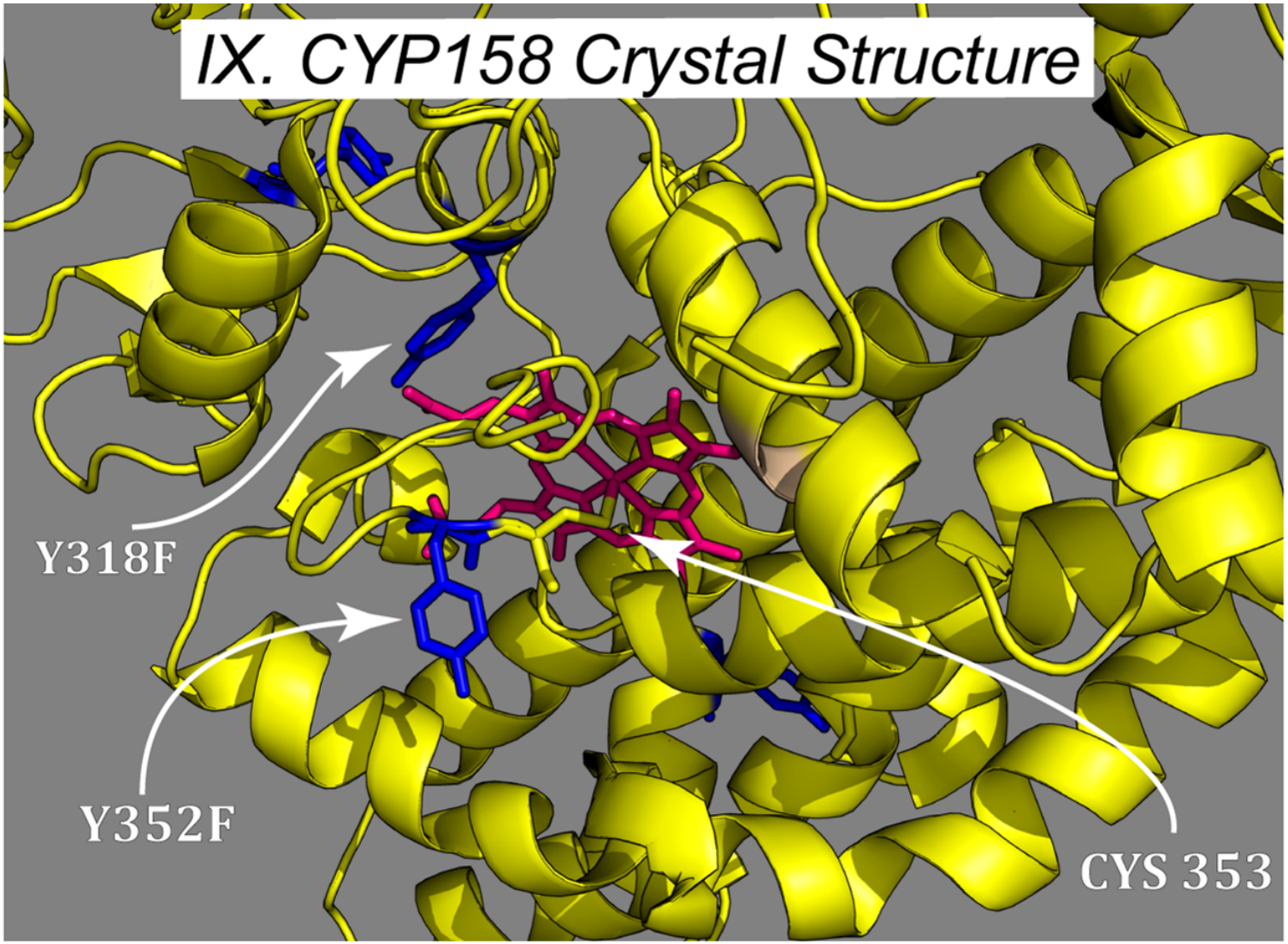

Fig S5: CYP158 crystal structure.(*27*, PDB accession code: 1S1F) The two arrows on the left designate the positions of tyrosine 352 and 318, both of which are ~ 10 Å away from the heme iron atom. Tyrosine 352 was changed to a phenyalanine in the CYP158 single variant. Both tyrosine 352 and 318 were changed to phenyalanine in the CYP158 double variant.

X. Stopped-Flow, Mössbauer, and EPR Spectra of CYP158 Single (Y352F) and Double (Y352F/Y318F) Variant Compound I (SV-I/DV-I)

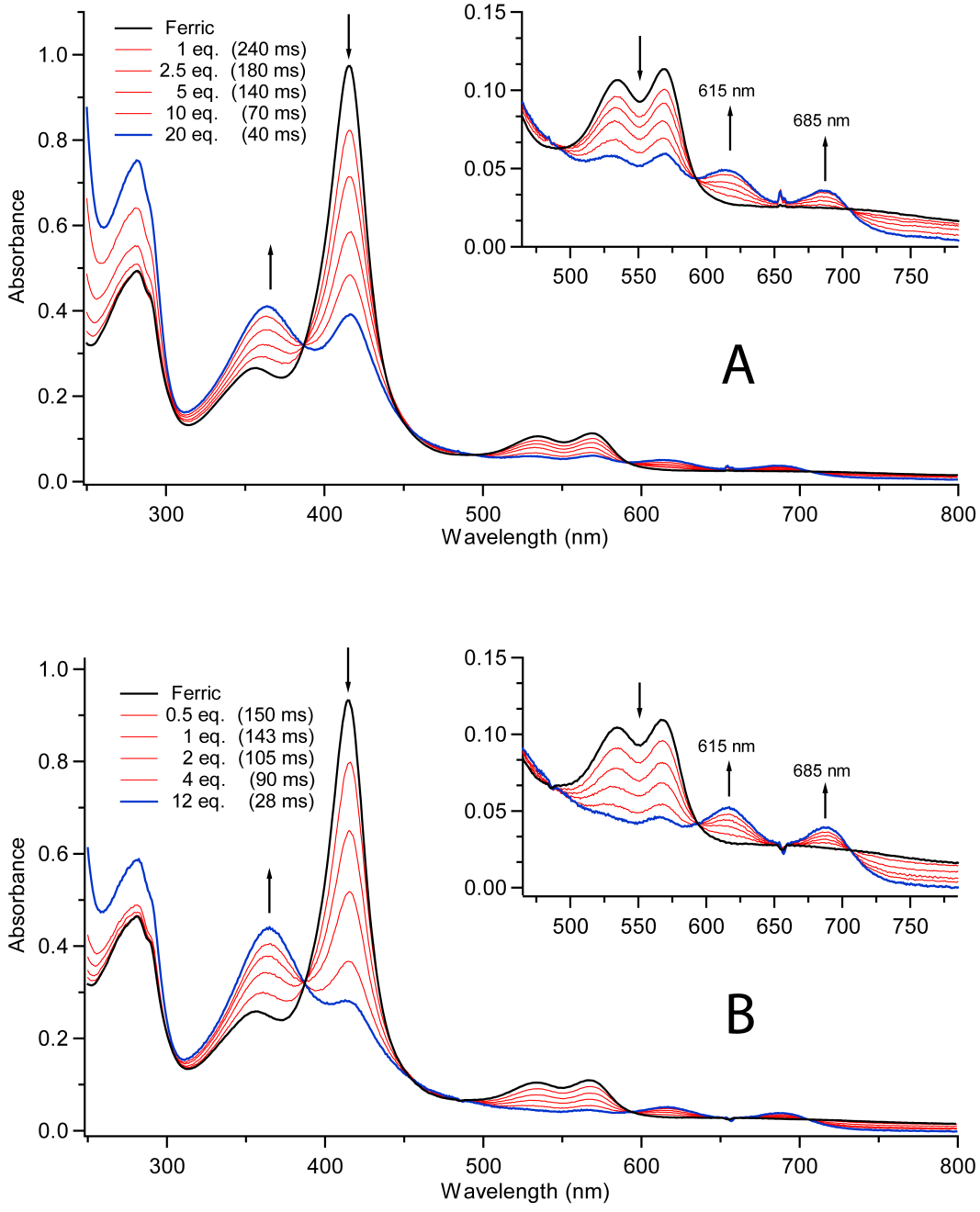

Figure S6: UV/visible spectra obtained from the stopped-flow mixing (1:1) of 20 μM ferric CYP158 SV **(A)** and DV **(B)** (100 mM tris-HCl, pH 7) with increasing equivalents of *m*-CPBA at 4°C. The formation rate and yield of compound I were found to scale with the equivalents of *m*-CPBA used for the reaction. All traces correspond to the max yield of compound I obtained at the corresponding time point. At later times, isosbestic points were lost, and a portion of the protein was degraded from the use of excess m-CPBA as judged by the final Reinheitszahl (R_z = $Abs_{416\ nm}/Abs_{280\ nm}$) ($R_z$). All spectral changes were completed within 2.5 s. The blue traces indicate ~ 80% yield for the single variant **(A)** and ~ 90% yield for the double variant **(B).**

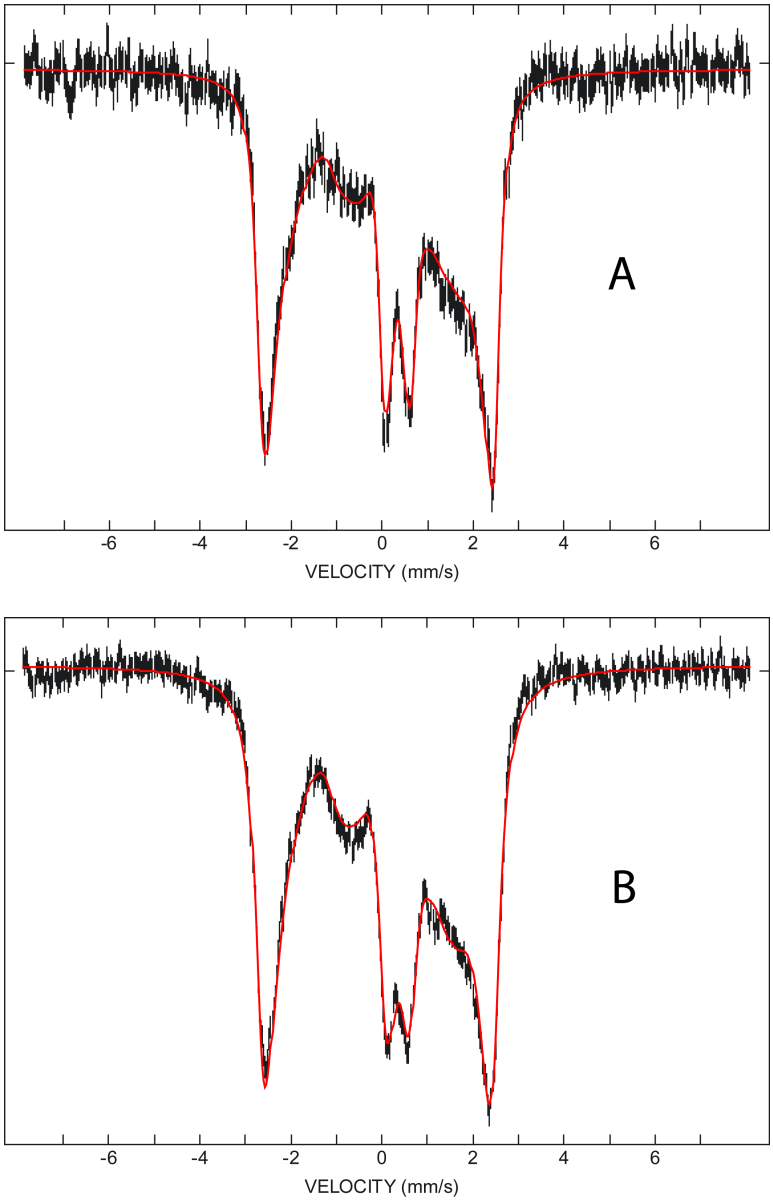

Figure S7: Mössbauer spectra of freezed-quenched CYP158 SV-I and DV-I samples. **A)** Spectrum of SV-I, obtained by subtracting the spectrum of ferric (15%) and compound II (3%) from the raw data. **B)** Spectrum of DV-I, obtained by subtracting the spectrum of ferric (15%) from the raw data. A 54-mT field was applied parallel to the γ-beam. The solid red line is the best fit of the data, assuming an effective S = 1/2 representation. Fit parameters are listed in Table S3. SV-I samples were prepared by reacting ferric protein (6 mM, Rz ≥ 2.00, in 100 mM tris-HCl buffer, pH 7.0) with a solution of m-CPBA (24 mM, 30% acetonitrile) in a 2:1 mixture (v/v). DV-I samples were prepared by reacting ferric protein (6 mM, Rz ≥ 2.00, in 100 mM tris-HCl buffer, pH 7.0) with a solution of m-CPBA (18 mM, 30% acetonitrile) in a 2:1 mixture (v/v).

Table S3: Mössbauer and EPR Parameters for CYP158 SV-I and DV-I. The intrinsic iron(IV)oxo hyperfine couplings were obtained by fitting the Mössbauer data in the coupled representation.

	σ	ΔE_Q	Effective S=1/2 Representation					
	(mm/s)	(mm/s)	g_x	g_y	g_z	A_x (T)	A_y (T)	A_z (T)
SV-I	0.13	0.90	2.02	1.99	1.93	-30	-32	2
DV-I	0.13	0.99	2.02	1.99	1.92	-30	-32	3

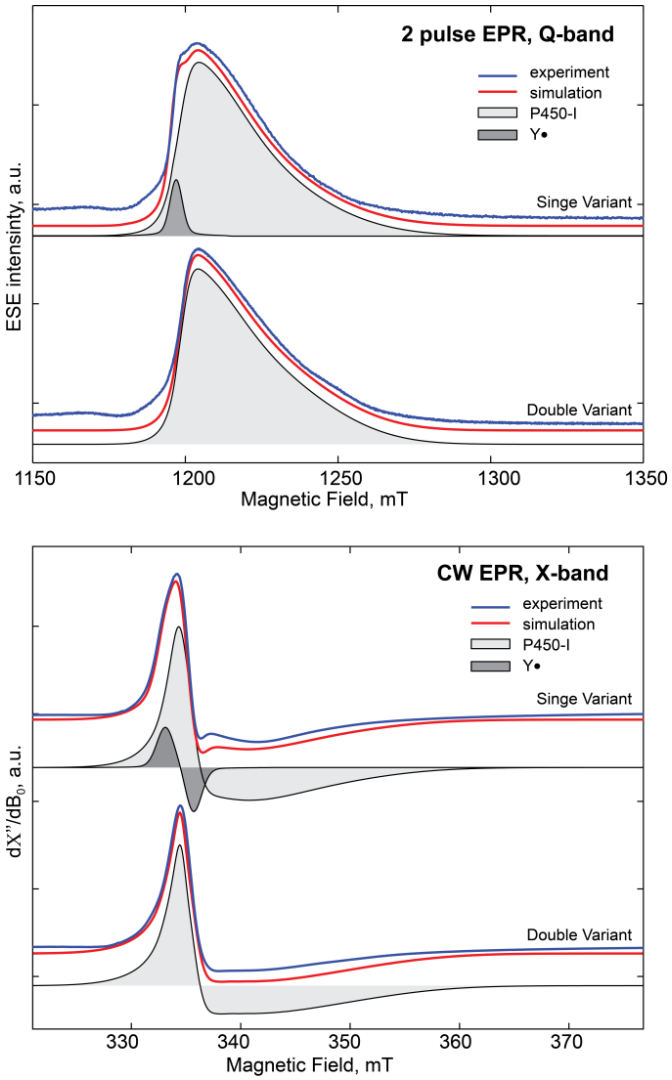

Figure S8: Difference in tyrosyl radical formation between CYP158 SV-I and DV-I as observed by low temperature EPR spectroscopy. Spectra were measured at 10K using Q-band 2 pulse EPR (top panel) and X-band continuous wave EPR (bottom panel) techniques. Simulations were performed using parameters presented in Table S4. Experimental conditions: **Q-band**: ν_{MW} = 33.616(SV)/33.621(DV) GHz, pulse sequence $[\pi/2]_{MW}$-τ-$[\pi]_{MW}$-τ-[signal], T(π/2)=24 ns, T(π)=40 ns, shot repetition time 200 ns; **X-band**: ν_{MW} = 9.3828 GHz (SV/DV), P_{MW} = 2.04 mW, Conversion time 40.96ms, time constant 40.96 ms, Modulation amplitude 10G.

Table S4: Simulation parameters used for interpretation of EPR spectra of single and double variant samples shown in figure F1.

	g-matrix				H strain (G)			composition**
	g_x	g_y	g_z		x	y	z	
SV-I	2.002	1.985	1.929	X:	1.42	8.4	13.3	94.82%
				Q:	5.3	20.9	44.7	94.85%
SV-I, Y• *	2.006	2.007	2.008	X:	-	-	-	5.18%
				Q:	-	-	-	5.15%
DV-I	2.002	1.987	1.921	X:	1.56	10.2	13.3	100%
				Q:	4.4	20.9	37.05	100%

*-g-values for the tyrosine radical are approximate. A ^{1}H hyperfine interaction was also included into the simulation with principal HF coupling constants : Ax= 32 MHz, Ay=38 MHz, Az=38 MHz.
**- composition was estimated as percent of area under absorption spectra.

XI. L316Y CYP119 Variant Compound II (CYP119V-II) Stopped-Flow, Mössbauer, and pKa Curve

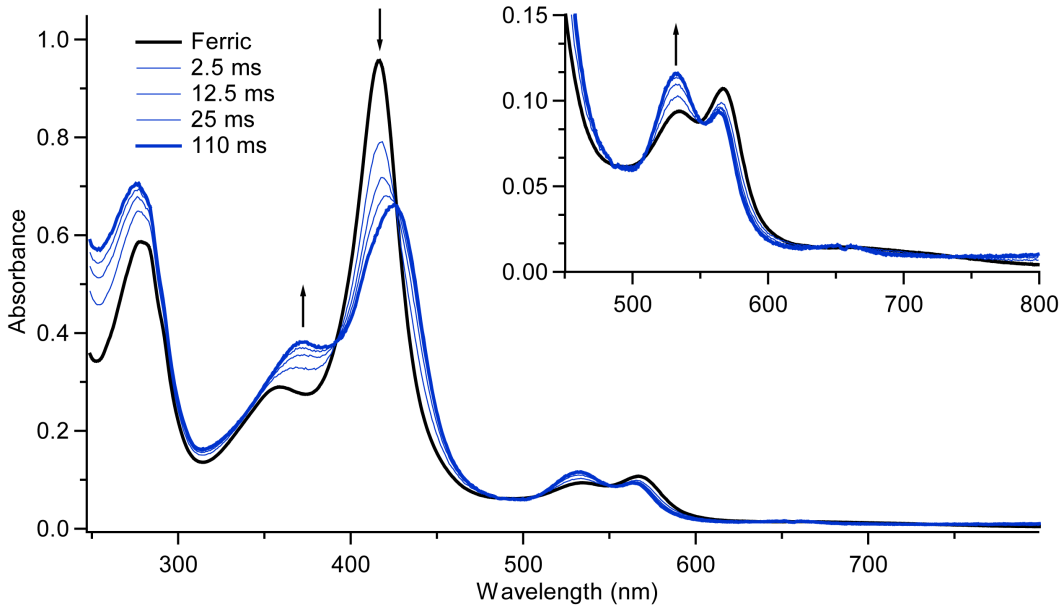

Figure S9: UV/visible spectra obtained from the stopped-flow mixing (1:1) of 20 µM ferric CYP119V (100 mM tris-HCl, pH 8) with 40 µM *m*-CPBA at 4°C. The blue traces correspond to spectra taken at 2.5, 12.5, 25, and 110 ms after mixing. Maximum yield of compound II was at ~ 110 ms. At later times, isosbestic points were lost, and a portion of the protein was degraded from the use of excess *m*-CPBA as judged by the final Reinheitszahl (Rz = $Abs_{416\ nm}/Abs_{280\ nm}$) (Rz). There was no observable compound I formation.

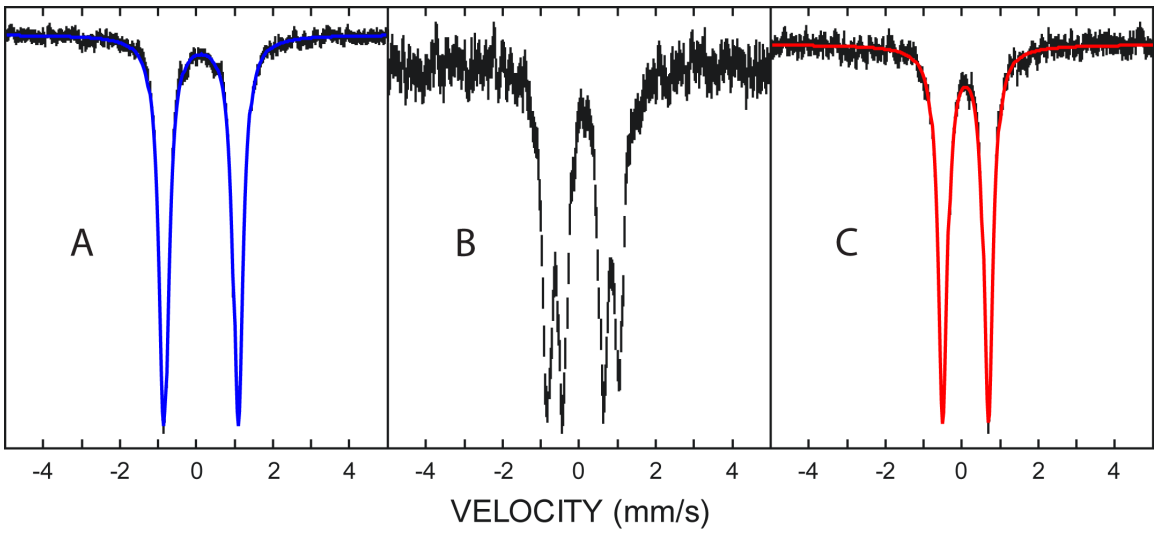

Figure S10: Mössbauer spectra of CYP119V-II at varying pH. (A) pH 8.0 (B) pH 11.8 (C) pH 13.6. The contribution from ferric enzyme (~20-35%) was subtracted from each spectrum. The isomer shift/quadrupole splitting parameters are 0.12/1.94 mm/s and 0.10/1.19 mm/s for the CYP119V-II hydroxide (A, blue) and oxo (C, red) intermediates respectively. Spectrum B is a 50:50 ratio of compound II hydroxide/oxo. Samples were prepared using a three syringe, double mix setup. Ferric CYP119V (3 mM) was reacted with *m*-CPBA (30 mM) in a 2:1 mixture (v/v) to form compound II hydroxide. CYP119V was in tris-HCl buffer (20 mM, pH 8) and *m*-CPBA was in a 40% solution of acetonitrile/water (v/v). Compound II hydroxide was then reacted in a subsequent 3:1 mixture with an arginine HCl/sodium hydroxide buffer (pH 14). The strength of the buffer was varied (10 mM – 108.16 mM) to change the final pH of the solution. The reaction was quenched in a liquid ethane bath 7 ms after the initial formation of compound II. Portions of the quenched samples were set aside to confirm the final pH of the solution. Samples were packed into Mössbauer sample cups for spectroscopic analysis at a final protein concentration of 1.5 mM. The final concentration of *m*-CPBA and acetonitrile were 7.5 mM and 10% (v/v) respectively.

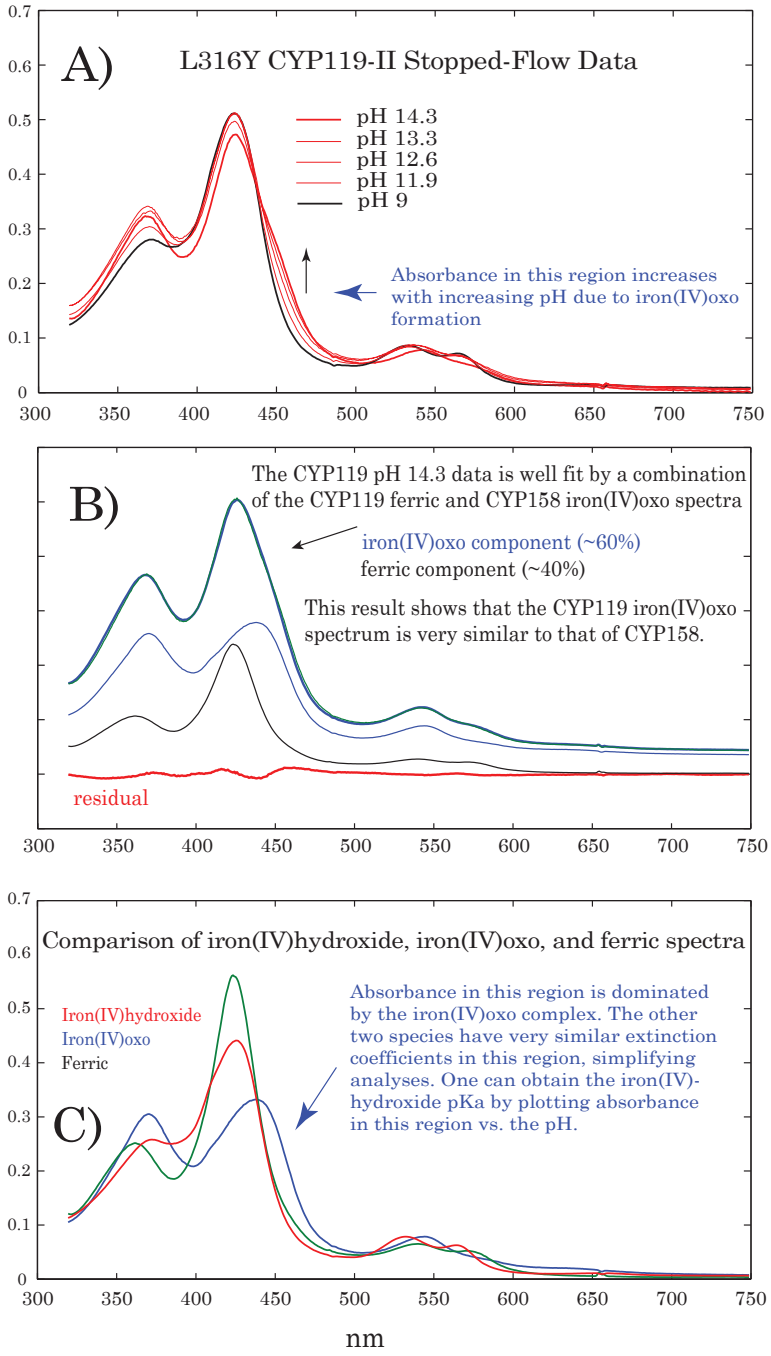

Figure S11. A shows UV/visible spectra obtained from the stopped-flow mixing of CYP119V-II (pH 7.75) with high pH buffer. Samples were prepared in a double-mixing experiment at 4°C. 20 μM ferric CYP119V (10 mM Tris-HCl, pH 7.75) was first mixed with 100 μM *m*-CPBA and held until maximum formation of CYP119V-II was achieved (50 ms). This solution was then mixed with a strongly buffered solution (containing 200 mM phosphate, 200 mM carbonate, 200 mM borate, 25 mM arginine, pH adjusted with KOH) to obtain the desired final pH. Spectra were collected 2.5 ms after mixing. Samples are composed of predominantly three species: iron(IV)hydroxide, iron(IV)oxo, and high pH ferric enzyme. The amount of ferric enzyme increases with increasing pH, from ~20% at pH 9 to ~40% at pH 14.3. Since the concentrations of more than two species are changing, the UV/Visible spectra lack multiple isosbestic points. Growth of the iron(IV)oxo species can be tracked in the region around 450 nm. This can be seen from a comparison of the iron(IV)hydroxide, iron(IV)oxo, and ferric spectra shown in **C**. This comparison requires knowledge of all three spectra. The spectra of the iron(IV)hydroxide complex (pH 7) and the high pH ferric enzyme (pH 14.3) are known. The iron(IV)oxo spectrum is very similar to (i.e. well approximated by) that of the CYP158 intermediate. Indeed, **B** shows that the pH 14.3 data is well fit by a linear combination of the CYP119 ferric and CYP158 iron(IV)oxo spectra with only a small residual. **C** shows a comparison of all three spectra. As noted previously, the iron(IV)oxo complex dominates the absorbance in the region around ~450 nm. Additionally, the iron(IV)hydroxide and ferric species have very similar extinction coefficients in this region simplifying analyses. Plotting the change in absorbance vs pH yields a pKa value of 12.2 (See Figure S12).

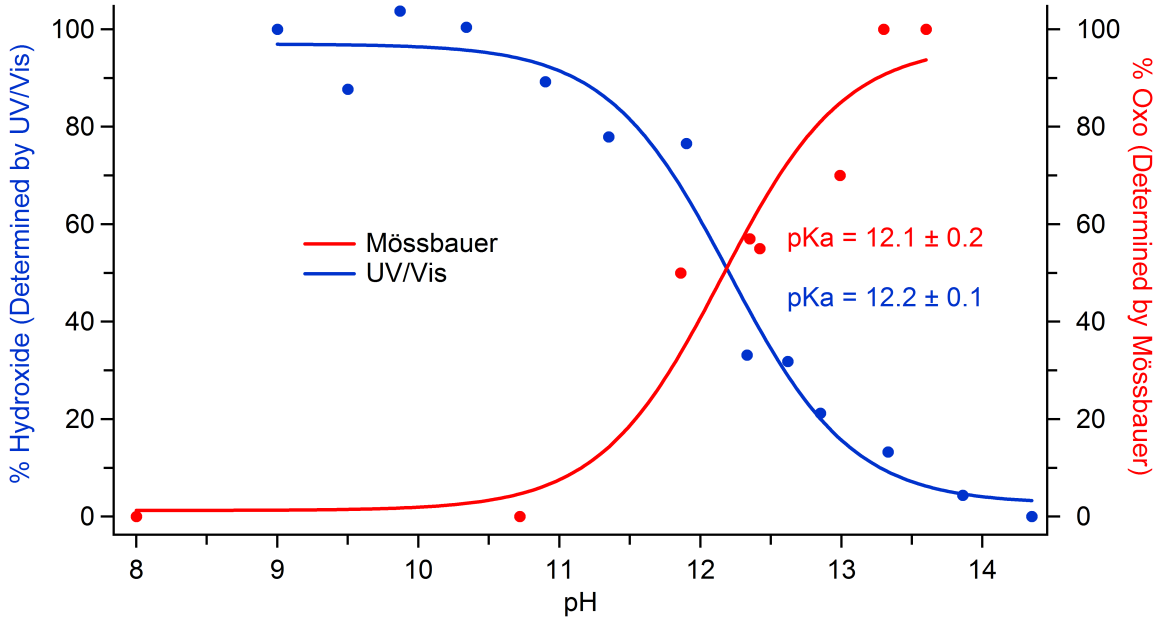

Figure S12: pH titration curves for CYP119V-II. Data obtained from stopped-flow UV/Visible (blue) and Mössbauer spectroscopies (red) yield pKa's of 12.2 and 12.1, respectively. The measured pKa is in good agreement with the value determined for CYP158-II (11.9).

XII. Effect of Tyrosine Radical on the Iron(IV)hydroxide pKa as a Function of Dielectric Constant

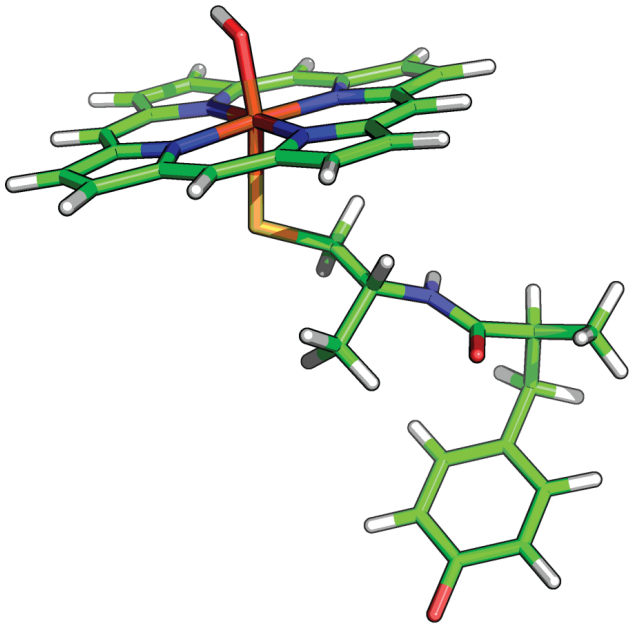

Change in iron(IV)hydroxide pKa upon tyrosine oxidation

ε	ΔpKa
80 (water)	-0.1
4.7	-0.3
4.0	-0.3
2.6	-0.5
1.0 (vacuum)	-2.3

The computational model shown was taken from the crystal structure of CYP158.(*27*) The geometry of the $CH_2SFeO(H)$ unit and the tyrosine were allowed to optimize (the CH2 of the tyrosine was fixed). Everything else was locked in place. Energies for protonation of the iron(IV)oxo moiety with and without the tyrosine oxidized were determined. All calculations were performed with Gaussian 09 at the B3LYP/6-311G level,(*60*) using implicit solvation.

E(hydroxide) - E(oxo) = ΔE (for protonation of ferryl)

Δ pKa = ($\Delta E_{tyr\text{-}OH}$ - $\Delta E_{tyr\text{-}O\bullet}$) *27.2*23.06/1.37
.... (the numbers convert Hartrees -> to eVs -> kcals/mol -> pKa)

ΔE does not account for the solvated H+, but the energy of the solvated H+ is the same in both cases. So, the subtraction cancels it out.

The solvated Tyr-O• does not affect the iron(IV)hydroxide pKa.

Figure S13: Effects of a tyrsoine radical on the iron(IV)hydroxide pKa of CYP158-II.